Life Sciences 236 (2019) 116939

Contents lists available at ScienceDirect

Life Sciences

journal homepage: www.elsevier.com/locate/lifescie

# 5,7,3′,4′-flavan-on-ol (taxifolin) protects against acetaminophen-induced liver injury by regulating the glutathione pathway

Cheng Hu[a,1], Jiawen Ye[b,1], Licong Zhao[c,1], Xiulong Li[a], Yu Wang[a], Xinhua Liu[a], Lingyun Pan[a], Lisha You[d], Long Chen[a,***], Yiqun Jia[a,**], Jiaqi Zhang[a,*]

[a] Experiment Center for Science and Technology, Shanghai University of Traditional Chinese Medicine, Shanghai, 201203, China
[b] Department of Cardiology, Shanghai Ninth People's Hospital, Shanghai Jiaotong University School of Medicine, Shanghai, 200011, China
[c] China Medical University, Shenyang, Liaoning, 110011, China
[d] School of Pharmacy, Shanghai University of Traditional Chinese Medicine, Shanghai, 201203, China

ARTICLE INFO

*Keywords:*
Metabolomics
Acetaminophen
Taxifolin
Liver protection
Oxidative stress injury
Glutathione

ABSTRACT

Taxifolin (TAX) reportedly exerts protective and therapeutic effects in liver. Herein, the effects of TAX against acetaminophen (APAP)-induced hepatotoxicity were investigated. Pharmacodynamics, pharmacology and metabolomics analyses of TAX were assessed on C57 mice and L-02 cells. TAX was administered for 7 days, and APAP was given on the last day to establish an acute liver injury model. ALT and AST levels were determined, and liver ROS, MDA, GST, GSH and GPX1 were analysed. The expression and protein abundance of GPX1, GPS-Pi, GCLC and GCLM were assessed by PCR and western blotting, and metabolic changes in cells and serum were investigated by UPLC-Q-Orbitrap-MS. Serum ALT and AST, and liver ROS, MDA, GST, GSH and GPX1 levels confirmed the protective effects of TAX. Besides, we found Only treating with TAX decreased the expression of CYP2E1 in mice liver tissue. TAX reversed the APAP-induced decrease in cell viability in L-02 cells, and reduced cellular ROS levels. Furthermore, TAX reversed the APAP-induced decrease in antioxidant enzymes at both mRNA and protein levels. Metabolomics analysis identified metabolites mainly related to glutathione metabolism (36 *in vivo* and 23 *in vitro*). The concentration of glutathione, oxidized glutathione, carnitine, succinic acid, pyroglutamic acid, citrulline, taurine, palmitoleic acid, phytoshingosine-1-P and sphingosine-1-P were close to normal levels after treating with TAX. These results indicate that TAX prevents APAP-induced liver injury by inhibiting APAP metabolic activation mediated by CYP450 enzymes, modulating glutathione metabolism, and expression of related antioxidative signals. These properties could be harnessed to prevent or treat hepatotoxicity.

## 1. Introduction

5,7,3′,4′-flavan-on-ol (taxifolin, TAX) is widely found in plants such as *Cedrus deodara*, *Larix sibirica* and *Taxus chinensis var. mairei* [1], as well as conifers including Siberian larch, *Pinus roxburghii*, *Cedrus deodara* and Chinese yew. Due to the presence of electron-donating hydroxyl groups at C-5 and C-7 on the A ring and C-3′ and C-4′ on B ring (Fig. 1A), TAX can readily scavenge free radicals. Recent research showed that TAX has anti-oxidation, hepatoprotective, anti-cancer, anti-inflammatory and various other pharmacological activities [2]. TAX can also prevent diabetic cardiomyopathy [3], acute pancreatitis [4] and liver toxicity [5–7] by inhibiting oxidative stress [8,9].

Acetaminophen (APAP) is a widely-used medicine for treating antipyretic analgesia. It is generally safe at low doses [10], but a high dose can result in acute liver failure (ALF). APAP is easy to overdose on when taken orally as a drug combination, which might be the main reason for drug-induced liver injury (DILI) [11,12]. Most APAP (> 90%) is excreted by glucuronidation and sulfation pathways, and some is metabolised to form N-acetyl-p-benzoquinoneimine (NAPQI) by liver cytochrome P450 (CYP450) enzymes [13]. Excessive NAPQI may deplete cellular glutathione (GSH) in liver, leading to liver injury induced by oxidative stress [14,15]. Traditional clinical indicators such as alanine aminotransferase (ALT) are commonly used to assess the severity of APAP-induced liver toxicity, but there is a delay between intake of

* Corresponding author.
** Corresponding author.
*** Corresponding author.
*E-mail addresses:* 13621765696@163.com (L. Chen), yqjia1961@126.com (Y. Jia), zhangjiaqinelly@gmail.com (J. Zhang).
[1] These authors contributed equally to this work.

https://doi.org/10.1016/j.lfs.2019.116939
Received 3 September 2019; Received in revised form 25 September 2019; Accepted 4 October 2019
Available online 05 October 2019
0024-3205/ 

**Abbreviations**

| | |
|---|---|
| TAX | Taxifolin |
| APAP | acetaminophen |
| ALF | acute liver failure |
| DILI | drug-induced liver injury |
| NAPQI | N-acetyl-p-benzoquinoneimine |
| GSH | glutathione |
| ALT | alanine aminotransferase |
| AST | aspartate aminotransferase |
| ROS | reactive oxygen species |
| MDA | malondialdehyde |
| GSH | glutathione |
| GST | glutathione-S-transferase |
| GPX1 | glutathione peroxidase |
| il-18 | interleukin-18 |
| il-1β | interleukin-1β |
| FBS | fetal bovine serum |
| ELISA | enzyme-linked immunosorbent assay |
| HRP | horseradish peroxidase |
| LC-MS | liquid chromatography mass spectrometry |
| PCA | principal component analysis |
| OPLS-DA | orthogonal partial least squares discriminant analysis |
| VIP | variable importance in projection |
| GCL | glutamate cysteine ligase |

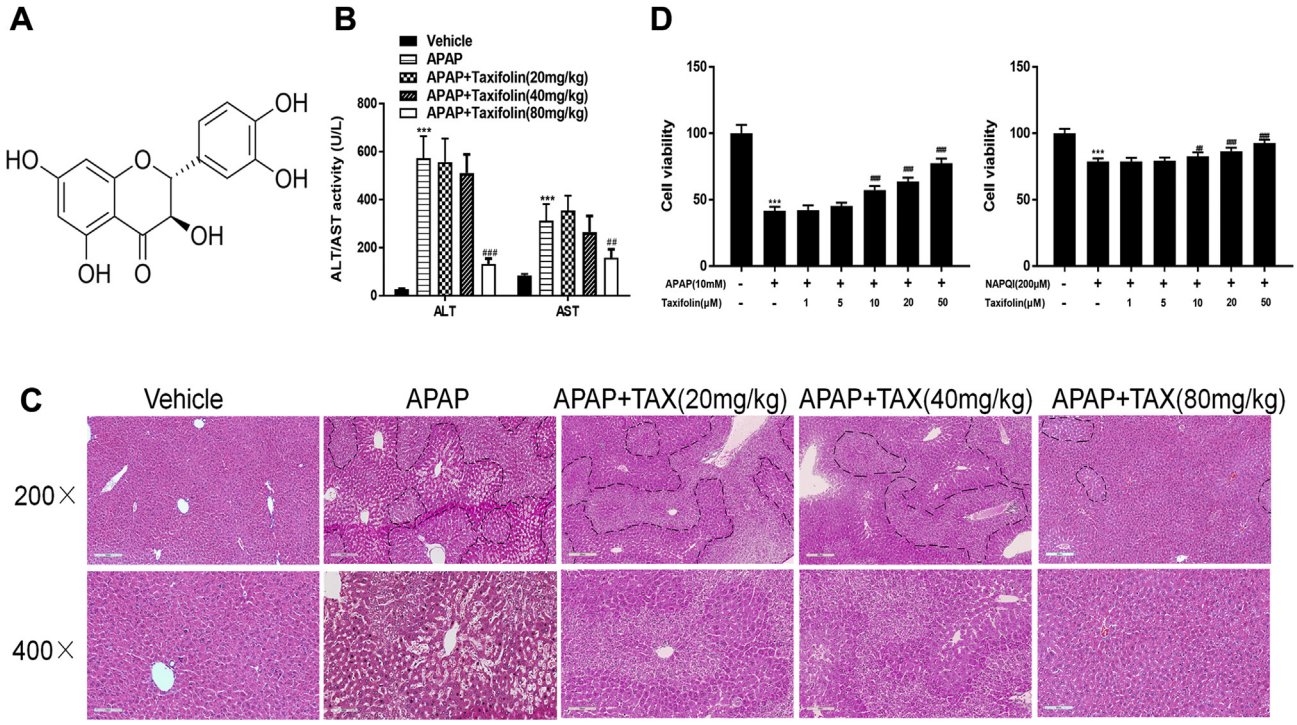


**Fig. 1.** TAX prevents APAP-induced liver injury in C57 mice and reduces APAP-induced cytotoxicity in L-02 cells. **(A)** Structure of TAX. The molecular formula of TAX is $C_{15}H_{10}O_6$ (molecular weight = 286.23). **(B)** Serum alanine aminotransferase (ALT) and aspartate aminotransferase (AST) activities. **(C)** Representative images of H&E-stained liver sections ( × 200 and × 400 magnification). Necrotic areas were identified by lack of nuclear staining or pyknotic nuclei and lines were marked along the boundaries. **(D)** Cytotoxicity assessment. Data are expressed as the means ± SEM (n = 8; $^{**}p < 0.01$, $^{***}p < 0.001$ compared to Control; $\#p < 0.05$, $\#\#p < 0.01$, $\#\#\#p < 0.001$ compared to APAP).

APAP and rising ALT levels. Patients may not be aware of APAP overdose, hence the discovery of new sensitive biomarkers may provide guidance for clinical practice.

Metabolomics technologies have the ability to detect potential biomarkers related to diseases, including liver injury [16–19]. Combined with clinical standards, such biomarkers may be valuable for predicting the severity of disease and patient recovery following treatment [20]. Metabolite analysis showed that glutathione, oxidative stress, fatty acids and the tricarboxylic acid cycle (TCA) are the main metabolic pathways affected by APAP [21–27].

In the present study, APAP was used to establish a model to test TAX as a protective medicine. Metabolomics approaches were employed to analyse abnormal metabolic biomarkers and thereby assess the therapeutic potential of TAX.

## 2. Material and methods

### 2.1. Reagents and chemicals

TAX (purity > 98.5%) was purchased from Meilune (Dalian, China). Kits for reactive oxygen species (ROS), malondialdehyde (MDA), glutathione (GSH), glutathione-S-transferase (GST), glutathione peroxidase (GPX1), interleukin-18 (il-18) and tumor necrosis factor-α (TNF-α) were purchased from Nanjing Jiancheng Bioengineering Institute (Nanjing, China). Lipofectamine RNAiMAX, 2′-7′-dichlorodihydrofluorescein diacetate ($H_2$ DCFDA), RPMI1640 and fetal bovine serum (FBS) were purchased from Life Technology (Carlsbad, CA). NE-PER nuclear, cytoplasmic extraction reagents, and a Pierce BCA Protein Assay Kit were purchased from ThermoFisher Scientific (Waltham, MA). A whole-cell protein extraction kit and enhanced chemiluminescence kit were obtained from Millipore (Darmstadt, Germany). PrimeScript RT Master Mix and SYBR Premix Ex Taq were bought from TaKaRa (Shiga, Japan). Antibodies for immunoblotting, including anti-

actin, -GPX1, GST-Pi, -GCLC, -GCLM, -CYP1A2, -CYP2E1, -CYP3A4 and -Keap1 were purchased from Cell Signaling Technology (Danvers, MA). Methanol and acetonitrile (HPLC grade) were purchased from Fisher Chemicals (Waltham USA). APAP was purchased from Sigma Chemical Co. (St. Louis, MO). Fenclonine was purchased from Aladdin (Shanghai, China).

### 2.2. Animals and treatments

C57BL/6 J mice (20 g ± 2) were purchased from the Shanghai Laboratory Animal Center of the Chinese Academy of Sciences (Shanghai, China). Experimental animals were treated with water and food *ad libitum*. Animals were fed at a constant temperature of 20–25 °C and humidity of 65 ± 5% with a 12 h light-dark cycle. All steps were completed in accordance with the Animal Management Rules of the Ministry of Health of the People's Republic of China, and were approved by the Animal Care Commission of Shanghai University of Traditional Chinese Medicine.

Twenty-four mice were divided randomly into three groups; (1) Control group (Vehicle), (2) Model group (APAP = 400 mg/kg) and (3) Treatment group (APAP = 400 mg/kg + TAX = 80 mg/kg). Vehicle group was given saline for 7 days as control. TAX (80 mg/kg) was given by i.g. administration for 7 days, and a single dose of APAP was given by i.g. at 1 h after administration of TAX on the final day. Mice were sacrificed by cardiac puncture, blood was withdrawn 4 h after administration of APAP, and plasma and liver were immediately collected for further study.

### 2.3. Cell culture and viability assay

The L-02 cell line was purchased from the Shanghai Institute of Cell Biology (Shanghai, China) and cultured in DMEM with FBS and 1% antibiotics. Cells were placed into 96-well plates at an initial density of 5,000 cells per well. After attachment, cells were treated with TAX for 15 min, and finally incubated with APAP for 24 h. After 500 μg/mL MTT was added to cells for 4 h, the resulting Formazan Blue was dissolved in 10% SDS, 5% isobutanol and 0.01 M HCl, and plates were scanned using a microplate reader (Thermo Scientific) at 570 nm, with 630 nm as a reference. Cell viability was standardised as the percentage of the control.

### 2.4. Blood and tissue biochemical analysis

A portion of each liver sample was fixed in 10% buffered formalin, paraffin sections were prepared, and H&E staining was applied to assess liver damage under a microscope. Blood samples were kept at room temperature for 2 h then centrifuged at 3000 rpm for 10 min to collect serum. ALT and AST were measured and liver ROS, MDA, GST, GSH and GPX1 were examined using commercial kits in accordance with standard protocols. Cell ROS, GSH and GST levels were also analysed using kits.

### 2.5. Enzyme-linked immunosorbent assay (ELISA)

The concentrations of inflammatory factors TNF-α and IL-18 in blood were examined by an ELISA kit according to the manufacturer's procedures.

### 2.6. Measurement of liver and cellular ROS

Cellular ROS was measured using a $H_2$DCFDA probe, as described previously [28]. To measure liver ROS levels, cold liver homogenate was centrifuged (10,000 g, 15 min, 4 °C), supernatants were incubated with 10 μM $H_2$DCFDA in the dark for 1 h, then transferred to a black-walled clear-bottomed 96-well plate. Fluorescence was immediately read at an excitation wavelength of 485–720 nm and an emission wavelength of 525–720 nm using a Synergy H4 spectrophotometer (BioTek, Winooski, VT). Protein concentrations in supernatants were assayed by BCA kits, calculated as units of fluorescence per microgram of protein, and presented as percentage of controls (% control).

### 2.7. Protein extraction and western blot analysis

A 50 μg sample of protein from lysed cells was separated by 10% SDS-PAGE, transferred to a nitrocellulose membrane, and blocked over 2 h. Membranes were incubated overnight with primary antibodies, followed by horseradish peroxidase (HRP)-conjugated secondary antibodies, and protein bands were visualised using ECL Plus Detection Reagent.

### 2.8. RNA isolation and quantitative real-time PCR

RNA was isolated from PTC cells using TRIzol, and cDNA was synthesised from 1 μg of total RNA in a 21 μl reaction volume using oligo dT18 primers and SuperScript reverse transcriptase. PCR amplification was carried out with Taq DNA polymerase using 1 μl of first-strand cDNA as templates. Thermal cycling was performed for 30 s at 94 °C, 30 s at 55 °C, and 30 s at 72 °C for 30 cycles, and relative expression levels were calculated by the $2^{-\Delta\Delta CT}$ method.

### 2.9. Metabolomics analysis

#### 2.9.1. Extraction and derivation of cell samples

Logarithmic growth phase cells were inoculated into 6-well plates at a density of $5 \times 10^5$ cells per well and treated according to the method described above. The following steps were performed: (1) after 24 h of culturing, the supernatant was discarded and cells were placed on ice; (2) cells were washed with 4 mL PBS, 2 mL of cold methanol was added to halt metabolism, and cells were collected by scraping; (3) cells were lysed sing a cell pulveriser for metabolite extraction, and samples were placed on ice for 20 min; (4) supernatants were transferred to an Eppendorf (EP) tube after centrifugation at 14,000 g for 10 min, then 10 μL DL-o-chlorophenylalanine (2.9 g/L, internal standard) was added. The supernatant was dried with nitrogen and the residue was stored at −80 °C; (5) the residue was reconstituted with 100 μL of methanol before analysis.

### 2.10. Preparation of serum samples

Serum samples (100 μL) were deproteinised using 400 μL of methanol containing internal standards (29 μg/mL DL-o-chlorophenylalanine). Samples were vortexed for 30s and centrifuged at 12,000 rpm at 4 °C for 15 min. A 200 μL sample of supernatant was transferred to a vial for analysis.

### 2.11. UPLC-Q-Orbitrap-MS analysis

Liquid chromatographic separation was achieved at a flow rate of 0.3 mL/min on an Hss T3 column (100 mm × 2.1 mm, 1.8 μm) using 0.1% formic acid (buffer A) and acetonitrile (buffer B). Gradient elution was performed as follows: 0–2 min, 95% A; 2–12 min, 5% A; 12–15 min, 5% A; 15–17 min, 95% A. MS data acquisition was completed using both positive and negative ionisation. Compounds were detected by full-scan mass analysis from 50 to 1000 *m/z* at a resolution of 60,000. Electrospray ionisation (ESI) parameters were as follow: Positive mode (1) heater temperature = 300 °C, (2) sheath gas flow = 45 arb (arbitrary units), (3) auxiliary gas flow = 10 arb, (4) sweep gas flow = 0 arb, (5) electrospray voltage = 3.8 kV, (6) capillary temperature = 350 °C, (7) S-LensF level = 30%; Negative mode (1) heater temperature = 300 °C, (2) sheath gas flow = 45 arb, (3) auxiliary gas flow = 5 arb, (4) sweep gas flow = 1 arb, (5) electrospray voltage = 3.2 kV, (6) capillary temperature = 350 °C, (7) S-LensF

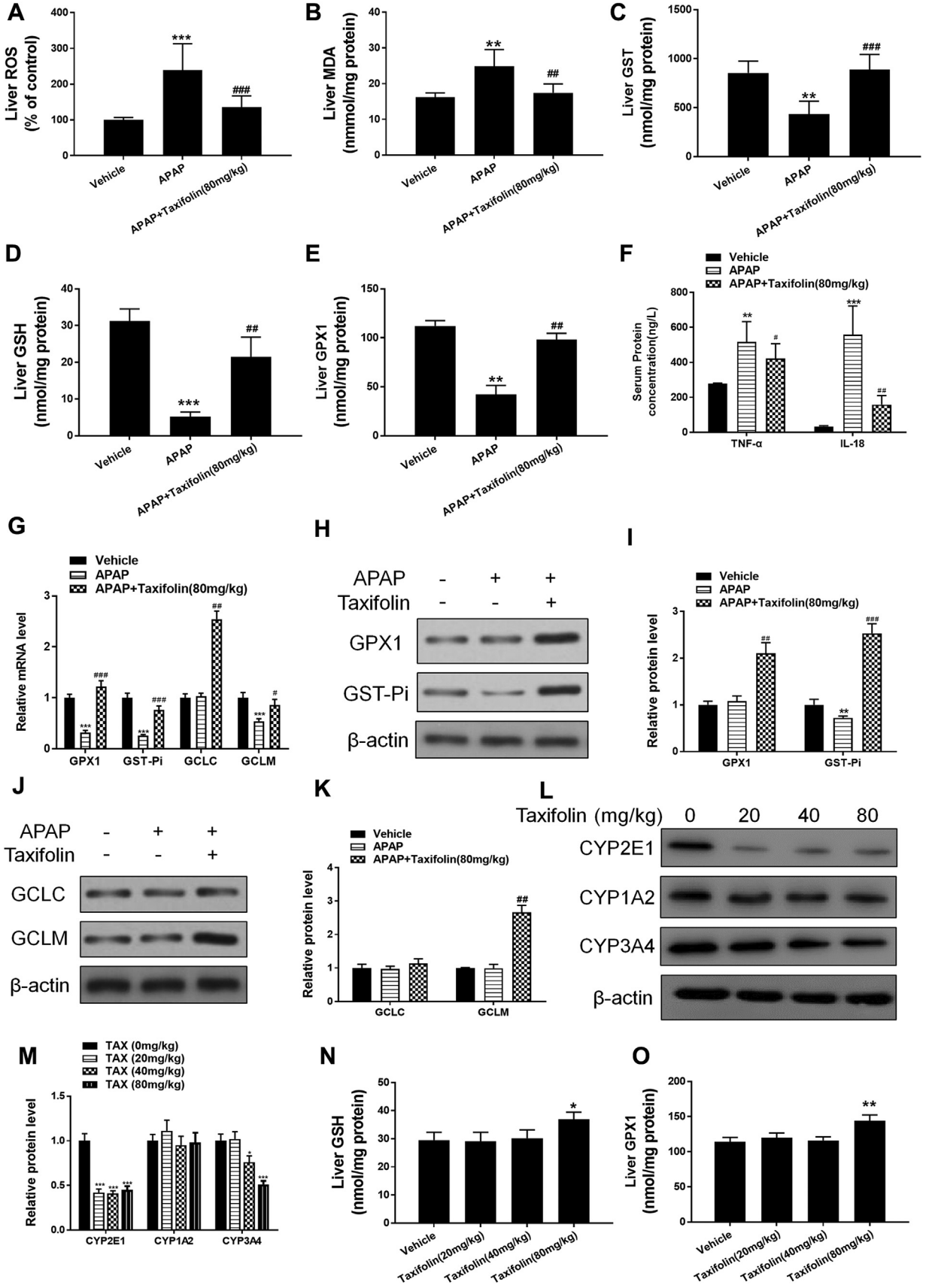


**Fig. 2.** TAX prevents APAP-induced liver oxidative stress in C57 mice. **(A)** Liver ROS levels. **(B)** Liver MDA levels. **(C)** Liver GST activity. **(D)** Liver GSH activity. **(E)** Serum GPX1 activity. **(F)** Serum concentrations of TNF-α and IL-18. **(G)** Liver mRNA expression of GPX1, GST-Pi, GCLC and GCLM determined by RT-PCR. **(H–M)** Western blotting analysis and quantified. **(K)** Liver GSH levels. **(L)** Serum GPX1 activity. Data are expressed as the means ± SEM (n = 8; $^{**}p < 0.01$, $^{***}p < 0.001$ compared to Control; $\#p < 0.05$, $\#\#p < 0.01$, $\#\#\#p < 0.001$ compared to APAP).

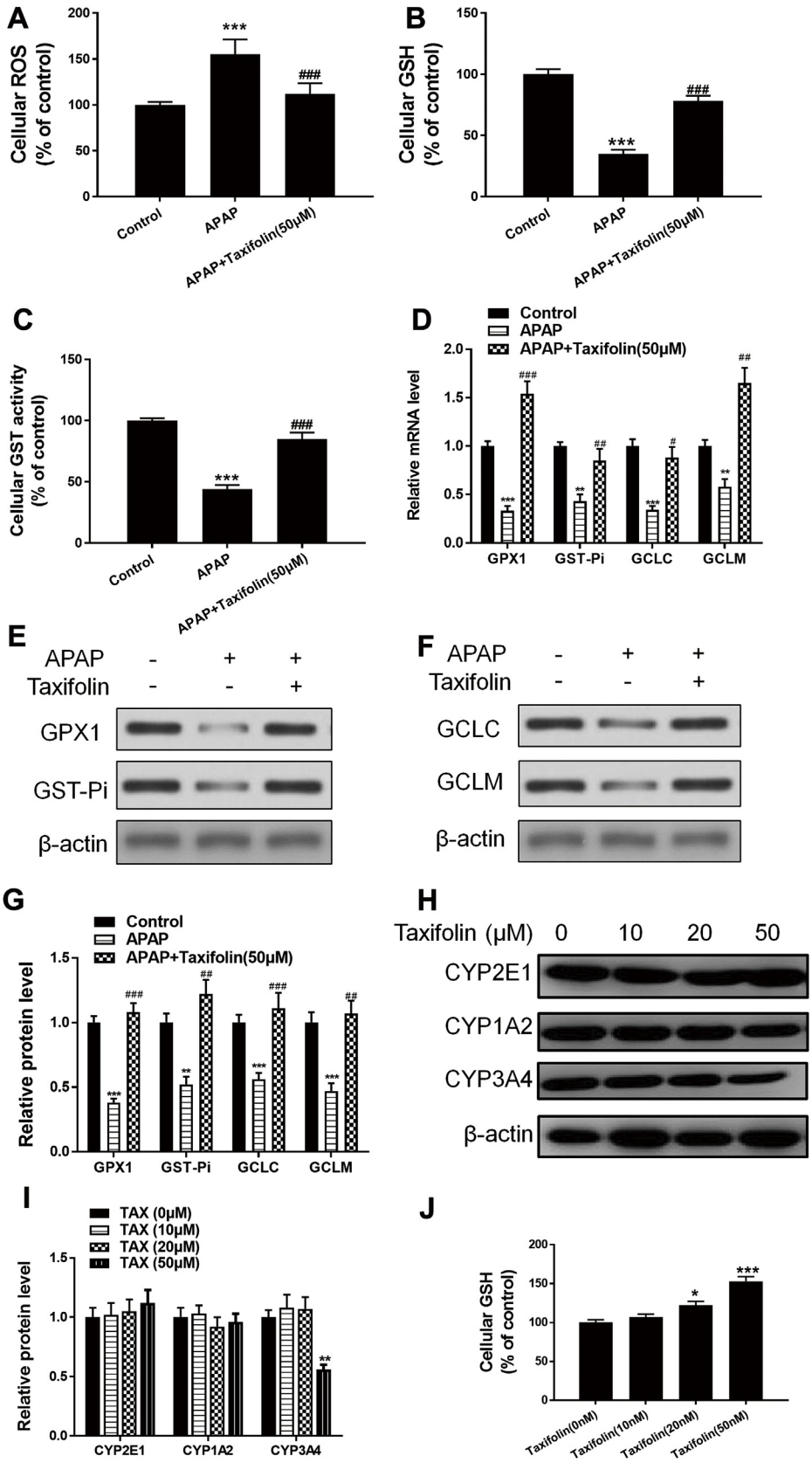


**Fig. 3.** TAX prevents APAP-induced liver oxidative stress in L-02 cells. **(A)** Cell ROS levels. **(B)** Cellular GSH levels. **(C)** Cellular GST activity. **(D)** mRNA expression of GPX1, GST-Pi, GCLC and GCLM determined by RT-PCR. **(E–I)** Western blotting analysis and quantified. **(H)** Cellular GSH levels. Data are expressed as the means ± SEM (n = 8; $^{**}p < 0.01$, $^{***}p < 0.001$ compared to Control; $\#p < 0.05$, $\#\#p < 0.01$, $\#\#\#p < 0.001$ compared to APAP).

level = 60%.

### 2.12. Metabolic data analysis

LC/MS data were extracted and pre-processed by Compound Discoverer 2.1 software (Thermo Company) and exported to generate a matrix including mass, retention time and peak intensity. Multivariate statistical analyses, including principal component analysis (PCA) and orthogonal partial least squares discriminant analysis (OPLS-DA) was performed on both serum and cell samples of mice in each group using SMICA-P software.

### 2.13. Metabolite identification and pathway analysis

Metabolites were identified according to accurate masses and product ion spectra by searching HMDB, KEGG and mzCloud databases. Metabolomic pathway analysis was performed using MetaboAnalyst 4.0.

### 2.14. Statistical analysis

SPSS 21.0 software was used to carry out t-tests among groups, and the data are expressed as the mean ± SEM. Differences were considered significant at $p < 0.05$.

## 3. Results

### 3.1. TAX prevents APAP-induced hepatotoxicity in vitro and in vivo

It is shown in Fig. 1B that APAP (400 mg/kg) induced an increase in ALT and AST in serum ($p < 0.001$), while TAX reversed the increase in ALT and AST ($p < 0.001$, $p < 0.01$). Additionally, H&E staining results (Fig. 1C) showed that severe liver damage occurred in the APAP (400 mg/kg) group, as evidenced by vacuolar degeneration, lymphocyte infiltration and intrahepatic haemorrhage. By contrast, in the APAP (400 mg/kg) + TAX (80 mg/kg) group, abnormal liver symptoms were rarely observed. As shown in Fig. 1D, APAP (10 mM) and NAPQI (200 μM), the metabolism product of APAP, decreased L-02 cell viability ($p < 0.001$), while TAX (10, 20, 50 μM) alleviated cytotoxicity induced by APAP in a dose-dependent manner ($p < 0.001$).

### 3.2. Effects of TAX on GSH and related enzymes in vivo

As shown in Fig. 2A and B, we found that TAX (80 mg/kg) reversed liver ROS and MDA elevation ($p < 0.001$, $p < 0.05$). Additionally, TAX increased the suppression of hepatic glutathione-S-transferase (GST), GSH and GPX1 induced by APAP ($p < 0.001$, $p < 0.01$, $p < 0.01$; Fig. 2C, D, E).

TNF-α and IL-18 levels were determined, and TAX both reversed the slight elevation in both compounds ($p < 0.001$, $p < 0.01$; Fig. 2F). Antioxidant enzymes (GPX1, GST-Pi, GCLC and GCLM) in mouse liver were assessed by RT-PCR and western blotting (Fig. 2G–K), since they are known to defend against endogenous ROS a participate in the glutathione pool. APAP decreased GPX1, GST-Pi and GCLM levels in liver ($p < 0.001$), but there was no significant change in GCLC. Following TAX treatment, levels of all antioxidant enzymes were increased ($p < 0.001$, $p < 0.001$, $p < 0.001$ $p < 0.05$).

It has been reported that CYP2E1, CYP3A4 and CYP1A2 are key cytochrome P450 (CYP) enzymes involved in APAP metabolism, and their metabolites may produce severe hepatotoxicity [29,30]. Western blot analysis was used to show that hepatic CYP2E1 and CYP3A4 expressions were significantly decreased in mice by TAX (80 mg/kg), while CYP1A2 underwent no obvious changes (Fig. 2L and M). Furthermore, we found that TAX (80 mg/kg) increased GSH and GPX1 concentrations in liver compared with the control group ($p < 0.05$, $p < 0.05$; Fig. 2N and O).

### 3.3. Effects of TAX on GSH and related enzymes in vitro

Cellular ROS, GSH and GST activities in L-02 cells were measured to assess the impact of TAX on oxidative stress damage. As shown in Fig. 3A, B and 3C, TAX significantly reversed the increase in cellular ROS, and decreased cellular GSH and GST induced by APAP ($p < 0.001$). Furthermore, mRNA and protein expression of antioxidant enzymes (GPX1, GST-Pi, GCLC and GCLM) in L-02 cells were also assessed (Fig. 3D–G), and all enzymes were decreased significantly

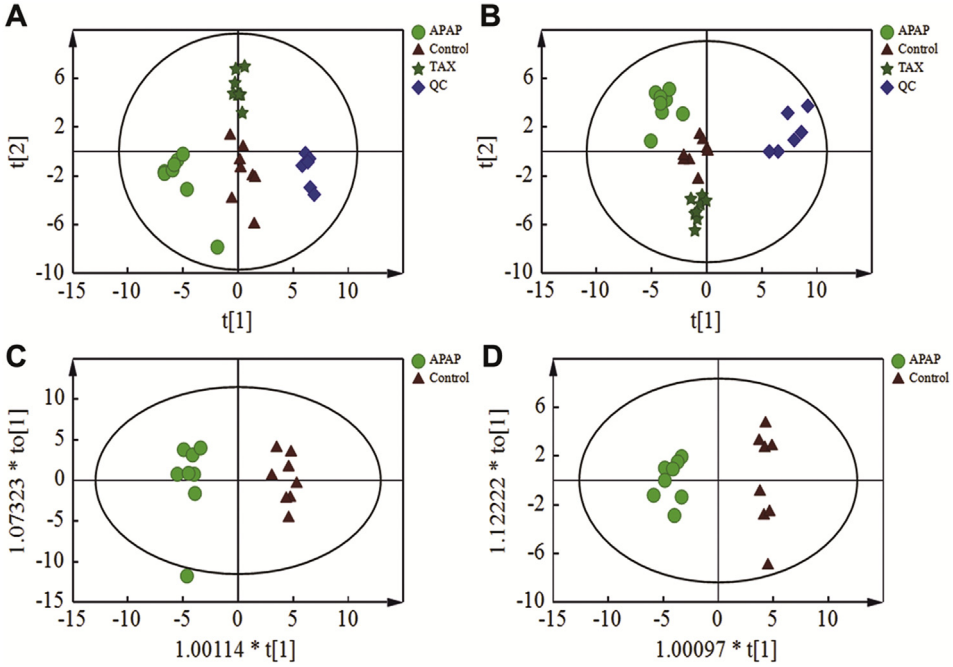


**Fig. 4.** PCA and OPLS-DA of cell metabolites (n = 8). **(A)** PCA score plot for negative mode data. **(B)** PCA score plot for positive mode data. **(C)** OPLS-DA score plot for negative mode data. **(D)** OPLS-DA score plot for positive mode data.

in the APAP group, but increased after TAX treatment ($p < 0.001$, $p < 0.01$, $p < 0.05$, $p < 0.01$). Western blot analysis showed that expression of CYP2E1 and CYP1A2 was no obvious changes while CYP3A4 was decreased by TAX after 24 h treatment (Fig. 3H and I). Besides, we found that TAX increased GSH levels in L-02 cells (Fig. 3J).

### 3.4. Metabolomics studies in vitro and in vivo

#### 3.4.1. Quality control of UPLC-MS data

QC samples were determined for instrument precision, and they clustered tightly on the PCA score plots for both positive and negative modes, separate from other groups. The PCA plots illustrated the stability of the UPLC-Orbitrap-MS system throughout the whole experiment.

### 3.5. PCA of APAP-induced liver injury

PCA was respectively performed on cell and serum samples in both positive and negative mode (Fig. 4). The $R^2X$ and $Q^2Y$ values of cell samples were 0.911 and 0.818 respectively in positive mode, and in negative mode they were 0.873 and 0.601. The $R^2X$ and $Q^2Y$ values of serum samples were 0.685 and 0.578, respectively, in positive mode, and in negative mode they were 0.671 and 0.348. These results indicate that the discriminative and predictive degree of the analytical model were satisfactory.

### 3.6. OPLS-DA of APAP-induced liver injury

OPLS-DA was employed on control and APAP group samples to identify potential differential metabolites. The $R^2Y$ and $Q^2Y$ values of cell samples were 0.911 and 0.818, respectively, in positive mode, and in negative mode were 0.999 and 0.996 (Fig. 5). The $R^2Y$ and $Q^2Y$ values of serum samples were 0.999 and 0.966, respectively, in positive mode, and in negative mode they were 0.888 and 0.646, respectively. These results indicate that the discriminative and predictive degree of the analytical model were satisfactory.

### 3.7. Identification of metabolites

Different metabolites were identified by OPLS-DA, and variable importance in projection (VIP > 1) and *p*-value ($p < 0.05$) were used for assessment. Finally, 36 different metabolites in serum samples and 23 different metabolites in cell samples were identified by searching against the library. According to the heatmap (Fig. 6), metabolites in the TAX treatment group tended to return to normal levels. To effectively visualise and characterise the protective effects of TAX against APAP, a heatmap representing the ratio of the concentration of metabolites in serum samples cell samples was produced. According to the heatmap (Fig. 6), metabolites in the TAX treatment group tended to be present at normal levels. The concentration of glutathione, carnitine, succinic acid and pyroglutamic acid in cell samples, and the concentration of citrulline, taurine, palmitoleic acid, phytoshingosine-1-P, sphingosine-1-P and oxidized glutathione in serum samples was similar to normal levels following TAX treatment.

### 3.8. Pathway analysis

Differential metabolites were analysed by MetaboAnalyst 4.0 to investigate metabolic pathways. Potential target metabolic pathways (impact value ≥ 0.10 and Rap *p*-value ≤ 0.05) in cell samples identified glutathione metabolism, and arginine and proline metabolism, while glutathione metabolism alone was identified in serum samples (Fig. 7). Metabolites in the two pathways included glutathione, oxidized glutathione, R-S-glutathione, L-pyroglutamic acid, spermidine, L-ornithine, citrulline and creatine. According to the KEGG and HMDB databases, these metabolites and enzymes are associated with various pathways, and metabolic networks are shown in Fig. 8.

## 4. Discussion

In this article, mice were sacrificed at 4 h after administration of APAP to assess the protective effects. In our previous study, mice were sacrificed at 2, 4 or 12 h to identify the time for APAP metabolism, *in vivo,* within 12 h. The results revealed minimal damage in mice sacrificed at 2 h. Therefore, mice were sacrificed at 4 h to study the protective effects of TAX on APAP-induced liver injury.

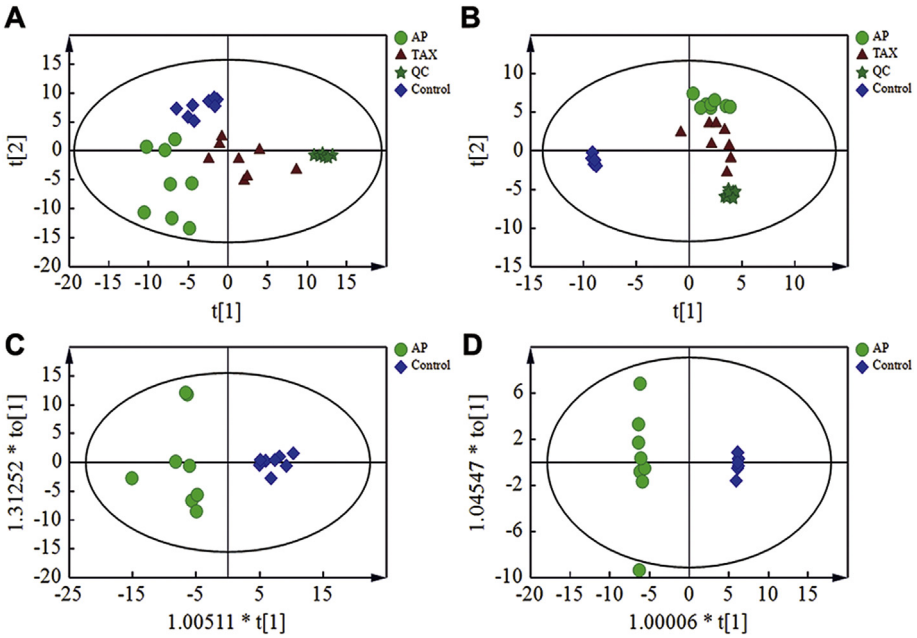


**Fig. 5.** PCA and OPLS-DA of serum metabolites (n = 8). **(A)** PCA score plot for negative mode data. **(B)** PCA score plot for positive mode data. **(C)** OPLS-DA score plot for negative mode data. **(D)** OPLS-DA score plot for positive mode data.

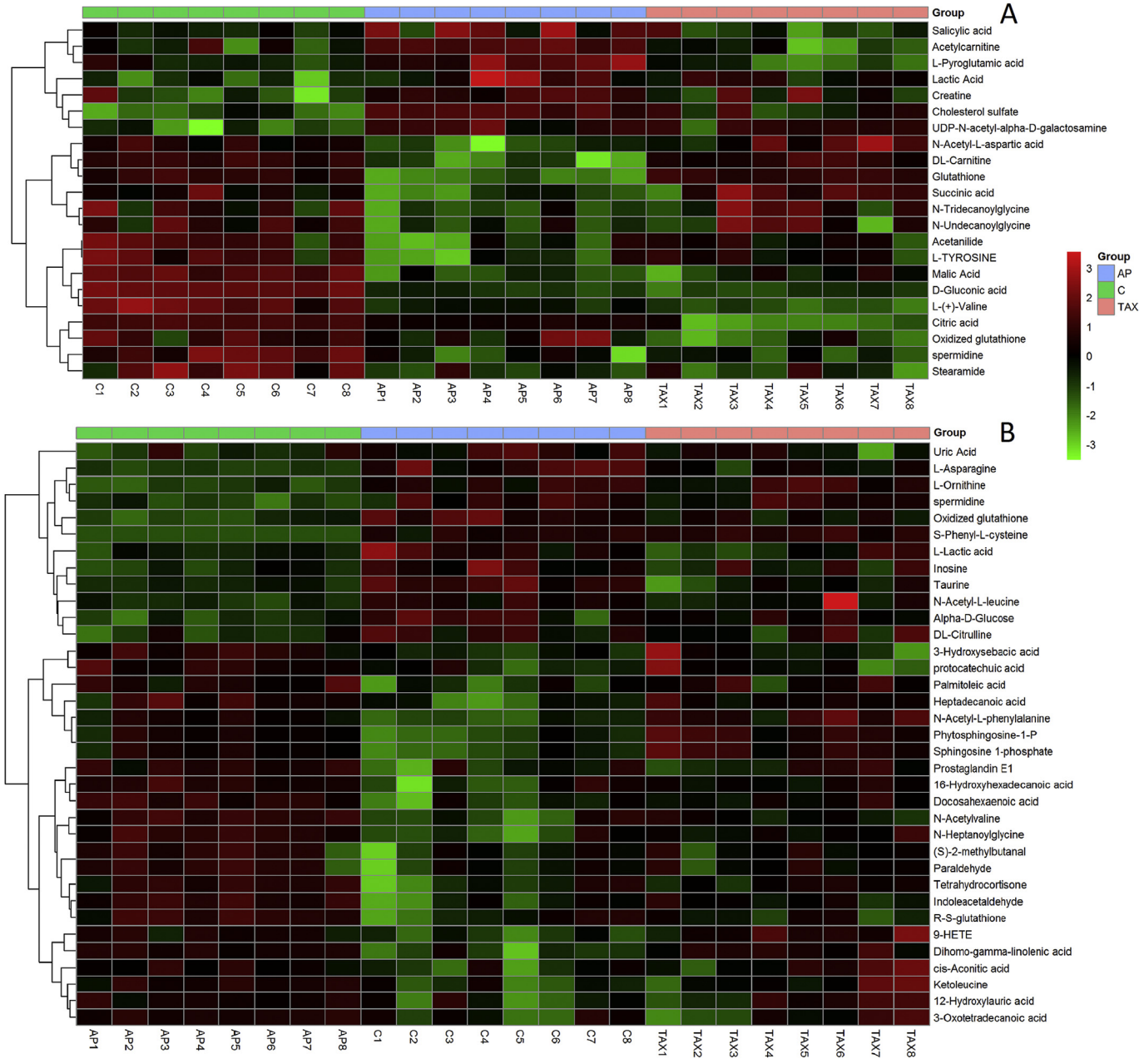


**Fig. 6.** Heatmap of TAX reversal of metabolite changes in L-02 cells and serum samples. **(A)** L-02 cells; **(B)** Serum from C57 mice (n = 8).

Like many other flavonoids, TAX exerts antioxidant effects [8,9,31,32]. The protective effects of TAX against APAP-induced ALF were first investigated herein, and the *in vitro* and *in vivo* results showed that TAX exerted strong liver protection activity. Specifically, it reversed the rise in ALT and AST in serum, as well as vacuolar degeneration, lymphocyte infiltration and intrahepatic haemorrhage in liver. Additionally, cell viability experiments showed the same trends. Thus, we believe that TAX exerts strong hepatoprotective effects against APAP-induced ALF.

GSH and its related enzymes were studied because they play important roles in detoxification of APAP. As mentioned in the introduction, Within the hepatocyte, APAP is metabolised to NAPQI by CYP450 enzymes. NAPQI (a metabolite of APAP) can deplete cellular GSH in the liver, and lead to oxidative stress-induced liver injury [14,15,33,34]. In our current study, the results showed TAX decreased CYP2E1 level which indicated the protective effect of TAX is through suppressing CYP2E1 activity and reduces the metabolic activation of APAP. Interestingly, TAX decreased CYP2E1 level in mice liver tissue while had no obvious change in L-02 cells. We think we should detect these enzymes levels in L-02 cells cultured in TAX for different times. What's more, different type of liver cells like Kupffer cells, hepatic stellate cells, liver sinusoidal endothelial cells and et al. should be concerned. What's more, Fig. 3D showed that NAPQI inhibited L-02 cell viability and TAX alleviated cytotoxicity induced by NAPQI. It indicated protective effect of TAX is not only through inhibiting metabolic activation. Hence, it's need to be further investigate how TAX plays a protective role in NAPQI-induced hepatotoxicity. Depleted GSH in the APAP group was reversed both *in vitro* and *in vivo*. Furthermore, ROS and MDA levels also showed that TAX alleviated oxidative stress injury in mice caused by APAP.

GPX1 is expressed in various tissues to protect cells against oxidative stress, and GSH serves as a reductant [35–37]. This enzyme catalyses the reduction of hydrogen peroxide and organic hydroperoxides [38]. GST activity is dependent on the continuous supply of GSH and

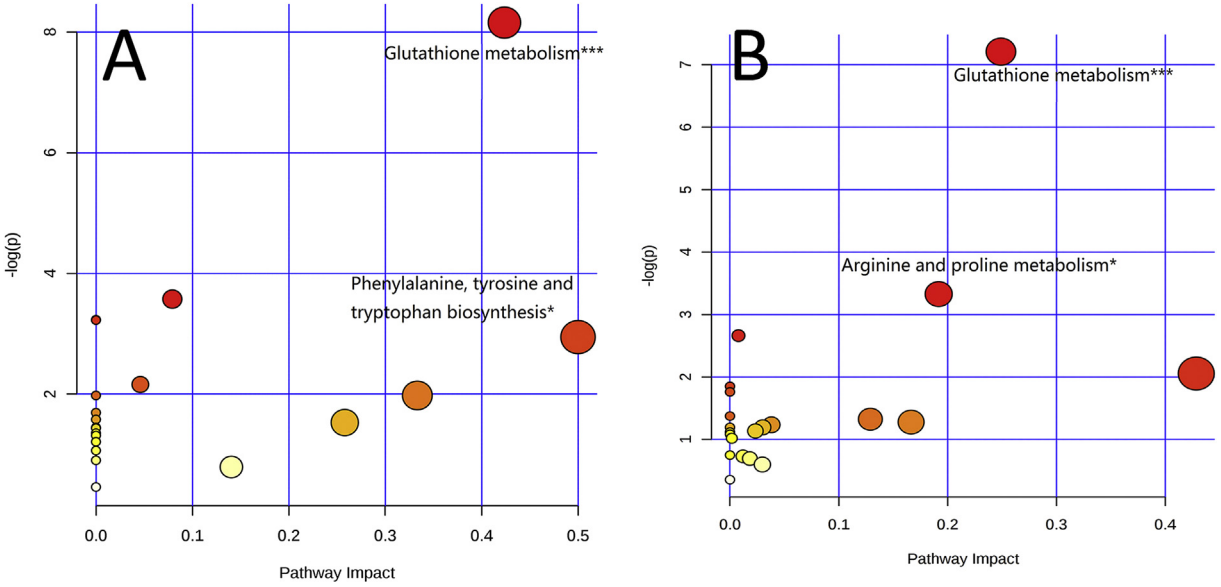


**Fig. 7.** Pathway-based enrichment analysis performed by Metaboanalyst 4.0. Pathway analysis of metabolites significantly altered between Control and APAP groups in **(A)** L-02 cells and **(B)** serum from C57 mice (***$p < 0.001$, **$p < 0.01$, *$p < 0.05$).

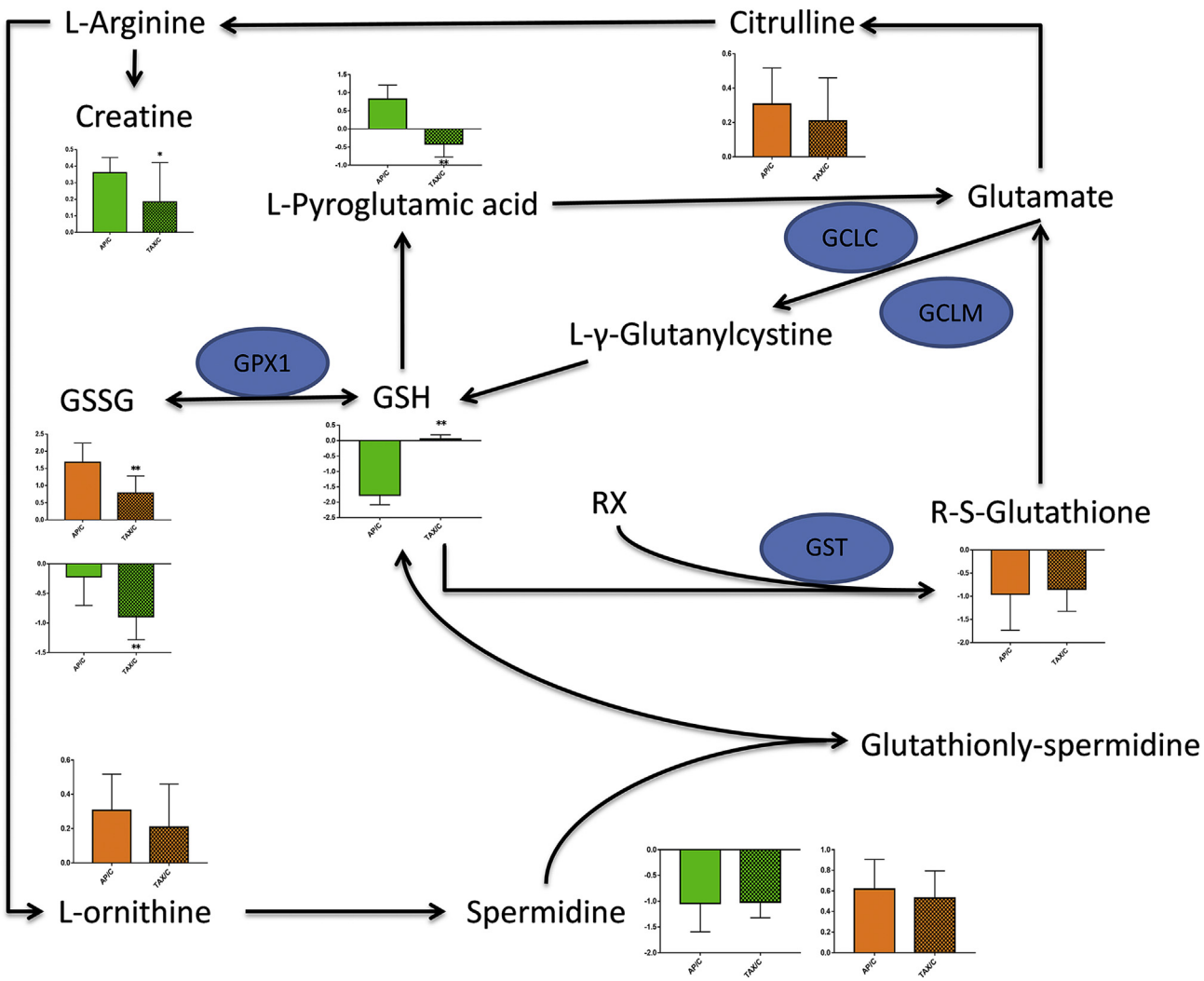


**Fig. 8.** Pathway map (serum data in orange and cells in green; ***$p < 0.001$, **$p < 0.01$, *$p < 0.05$). (For interpretation of the references to colour in this figure legend, the reader is referred to the Web version of this article.)

the elimination of GSSG from the cell. The main function of GST is to catalyse the nucleophilic attack of GSH on electrophilic carbon, sulphur and nitrogen atoms of nonpolar xenobiotic substrates, thereby preventing their interaction with crucial cellular proteins and nucleic acids [39,40]. NAPQI is a xenobiotic metabolite generated by overdose of APAP, and the activity of GST can indicate the toxicity of APAP, as well as the detoxification ability of TAX. According to the results for mouse liver samples and cells, similar trends in GPX1 and GST activities were observed, indicating that TAX exerted significant liver protective effects against oxidative stress injury caused by APAP.

Glutamate cysteine ligase (GCL) is the rate-limiting enzyme for GSH, and participates in improving oxidative stress ability. GCLC and GCLM are the catalytic and regulatory subunits of GCL, respectively [41–43]. Reduced levels of GCLC and GCLM may lead to low GSH content, and slow clearance of ROS. Therefore, mRNA and protein expression of antioxidative enzymes (GPX1, GST-Pi, GCLC and GCLM) were investigated. Reduced levels of GPX1, GST-Pi, GCLC and GCLM in cells and liver indicated serious oxidative injury in the APAP group, while expression levels in the TAX group were similar to the control group. However, GCLC did not differ significantly between Control and APAP groups *in vivo*, while expression rose significantly following TAX treatment. This may be because (1) regulation of GCLM and GCLC is independent, and (2) high expression of GCLC in the TAX group may be a protective phenomenon since TAX exerts antioxidant effects by up-regulating the expression of GCLC.

Metabolomics analysis of cells and serum were performed to verify the above results. PCA and OPLS-DA were applied to assess the metabolomics data. These methods are usually used to decrease the dimensionality of large complex datasets containing thousands of variables. Significant differential metabolites between Control and APAP groups identified by OPLS-DA (VIP > 1, $p < 0.05$) were analysed by Metaboanalyst 4.0. Glutathione metabolism in cells and serum were found to be abnormal (Fig. 7), while TAX reversed the abnormalities (Figs. 6 and 8). As shown in Fig. 8, the content of these metabolites followed similar trends to the expression of GCLC, GCLM, GPX1 and GST at both gene and protein levels (Figs. 2 and 3). Furthermore, TAX treatment decreased the content of GSSG and maintained GSH homeostasis.

## 5. Conclusion

The present results demonstrated that TAX protects against APAP-induced hepatotoxicity and oxidative stress by inhibiting metabolic activation mediated by CYP450 enzymes and helping to maintain glutathione homeostasis *in vivo* and *in vitro*.

## Author contributions

YJ and LC designed experiments; CH, JZ, LZ, MJ, XL, YW, XW and LP performed experiments and analysed the results; HC and JZ wrote the manuscript. LY and YJ revised and approved the submitted version.

## Declaration of competing interest

We declare that there are no conflicts of interest.

## Acknowledgements

This work was financially supported by the Budget of Experiment Center for Science and Technology (18LK022).

## References

[1] V.S. Rogovskii, A.I. Matiushin, N.L. Shimanovskii, A.V. Semeikin, T.S. Kukhareva, et al., [Antiproliferative and antioxidant activity of new dihydroquercetin derivatives], Eksp. Klin. Farmakol. 73 (2010) 39–42.

[2] F. Topal, M. Nar, H. Gocer, P. Kalin, U.M. Kocyigit, et al., Antioxidant activity of taxifolin: an activity-structure relationship, J. Enzym. Inhib. Med. Chem. 31 (2016) 674–683, https://doi.org/10.3109/14756366.2015.1057723.

[3] X. Sun, R.C. Chen, Z.H. Yang, G.B. Sun, M. Wang, et al., Taxifolin prevents diabetic cardiomyopathy in vivo and in vitro by inhibition of oxidative stress and cell apoptosis, Food Chem. Toxicol. : Int. J. Publ. Br. Ind. Biol. Res. Assoc. 63 (2014) 221–232, https://doi.org/10.1016/j.fct.2013.11.013.

[4] D. Du, L. Yao, R. Zhang, N. Shi, Y. Shen, et al., Protective effects of flavonoids from Coreopsis tinctoria Nutt. on experimental acute pancreatitis via Nrf-2/ARE-mediated antioxidant pathways, J. Ethnopharmacol. 224 (2018) 261–272, https://doi.org/10.1016/j.jep.2018.06.003.

[5] A.C. Akinmoladun, C.O. Oladejo, S.S. Josiah, C.D. Famusiwa, O.B. Ojo, et al., Catechin, quercetin and taxifolin improve redox and biochemical imbalances in rotenone-induced hepatocellular dysfunction: relevance for therapy in pesticide-induced liver toxicity? Pathophysiology : Off. J. Int. Soc. Pathophysiol. 25 (2018) 365–371, https://doi.org/10.1016/j.pathophys.2018.07.002.

[6] J.W. Kim, T.B. Kim, H.W. Kim, S.W. Park, H.P. Kim, et al., Hepatoprotective flavonoids in opuntia ficus-indica fruits by reducing oxidative stress in primary rat hepatocytes, Pharmacogn. Mag. 13 (2017) 472–476, https://doi.org/10.4103/pm.pm_232_16.

[7] H. Kuang, Z. Tang, C. Zhang, Z. Wang, W. Li, et al., Taxifolin activates the Nrf2 antioxidative stress pathway in mouse skin epidermal JB6 P+ cells through epigenetic modifications, Int. J. Mol. Sci. 18 (2017), https://doi.org/10.3390/ijms18071546.

[8] T.V. Arutyunyan, A.F. Korystova, L.N. Kublik, M. Levitman, V.V. Shaposhnikova, et al., Taxifolin and fucoidin abolish the irradiation-induced increase in the production of reactive oxygen species in rat aorta, Bull. Exp. Biol. Med. 160 (2016) 635–638, https://doi.org/10.1007/s10517-016-3236-2.

[9] C. Voulgari, D. Papadogiannis, N. Tentolouris, Diabetic cardiomyopathy: from the pathophysiology of the cardiac myocytes to current diagnosis and management strategies, Vasc. Health Risk Manag. 6 (2010) 883–903, https://doi.org/10.2147/VHRM.S11681.

[10] F.M. Russell, F. Shann, N. Curtis, K. Mulholland, Evidence on the use of paracetamol in febrile children, Bull. World Health Organ. 81 (2003) 367–372.

[11] M. Blieden, L.C. Paramore, D. Shah, R. Ben-Joseph, A perspective on the epidemiology of acetaminophen exposure and toxicity in the United States, Expert Rev. Clin. Pharmacol. 7 (2014) 341–348, https://doi.org/10.1586/17512433.2014.904744.

[12] W. Bernal, Changing patterns of causation and the use of transplantation in the United Kingdom, Semin. Liver Dis. 23 (2003) 227–237, https://doi.org/10.1055/s-2003-42640.

[13] E.M. Alonso, L.P. James, S. Zhang, R.H. Squires, Pediatric acute liver failure study, G. Acetaminophen adducts detected in serum of pediatric patients with acute liver failure, J. Pediatr. Gastroenterol. Nutr. 61 (2015) 102–107, https://doi.org/10.1097/MPG.0000000000000814.

[14] H. Jaeschke, M.R. McGill, A. Ramachandran, Oxidant stress, mitochondria, and cell death mechanisms in drug-induced liver injury: lessons learned from acetaminophen hepatotoxicity, Drug Metab. Rev. 44 (2012) 88–106, https://doi.org/10.3109/03602532.2011.602688.

[15] H. Jaeschke, T.R. Knight, M.L. Bajt, The role of oxidant stress and reactive nitrogen species in acetaminophen hepatotoxicity, Toxicol. Lett. 144 (2003) 279–288.

[16] J.K. Nicholson, J.C. Lindon, Systems biology: metabonomics, Nature 455 (2008) 1054–1056, https://doi.org/10.1038/4551054a.

[17] R. Bujak, W. Struck-Lewicka, M.J. Markuszewski, R. Kaliszan, Metabolomics for laboratory diagnostics, J. Pharm. Biomed. Anal. 113 (2015) 108–120, https://doi.org/10.1016/j.jpba.2014.12.017.

[18] M. Yu, S. Sun, J. Yu, F. Du, S. Zhang, et al., Discovery and validation of potential serum biomarkers for pediatric patients with congenital heart diseases by metabolomics, J. Proteome Res. 17 (2018) 3517–3525, https://doi.org/10.1021/acs.jproteome.8b00466.

[19] L. Zhao, J. Zhang, L. Pan, L. Chen, Y. Wang, et al., Protective effect of 7,3',4'-flavon-3-ol (fisetin) on acetaminophen-induced hepatotoxicity in vitro and in vivo, Phytomedicine : Int. J. Phytother. Phytopharm. 58 (2019) 152865, https://doi.org/10.1016/j.phymed.2019.152865.

[20] K.W. Jordan, J. Nordenstam, G.Y. Lauwers, D.A. Rothenberger, K. Alavi, et al., Metabolomic characterization of human rectal adenocarcinoma with intact tissue magnetic resonance spectroscopy, Dis. Colon Rectum 52 (2009) 520–525, https://doi.org/10.1007/DCR.0b013e31819c9a2c.

[21] H. Wang, Z. He, Y. Zhang, J. Zhang, (1)H NMR metabolic signature of cerebrospinal fluid following repetitive lower-limb remote ischemia preconditioning, Neurochem. Int. 116 (2018) 95–103, https://doi.org/10.1016/j.neuint.2018.02.009.

[22] B.S. Kumar, B.C. Chung, O.S. Kwon, B.H. Jung, Discovery of common urinary biomarkers for hepatotoxicity induced by carbon tetrachloride, acetaminophen and methotrexate by mass spectrometry-based metabolomics, J. Appl. Toxicol. : JAT 32 (2012) 505–520, https://doi.org/10.1002/jat.1746.

[23] M. Kyriakides, L. Maitre, B.D. Stamper, I. Mohar, T.J. Kavanagh, et al., Comparative metabonomic analysis of hepatotoxicity induced by acetaminophen and its less toxic meta-isomer, Arch. Toxicol. 90 (2016) 3073–3085, https://doi.org/10.1007/s00204-015-1655-x.

[24] T. Yamamoto, K. Tomizawa, M. Fujikawa, Y. Sato, H. Yamada, et al., Evaluation of human hepatocyte chimeric mice as a model for toxicological investigation using panomic approaches–effect of acetaminophen on the expression profiles of proteins and endogenous metabolites in liver, plasma and urine, J. Toxicol. Sci. 32 (2007) 205–215.

[25] M.R. McGill, H. Jaeschke, Mechanistic biomarkers in acetaminophen-induced hepatotoxicity and acute liver failure: from preclinical models to patients, Expert Opin. Drug Metabol. Toxicol. 10 (2014) 1005–1017, https://doi.org/10.1517/

17425255.2014.920823.
[26] J.W. Ko, S.H. Park, N.R. Shin, J.Y. Shin, J.W. Kim, et al., Protective effect and mechanism of action of diallyl disulfide against acetaminophen-induced acute hepatotoxicity, Food Chem. Toxicol. : Int. J. Publ. Br. Ind. Biol. Res. Assoc. 109 (2017) 28–37, https://doi.org/10.1016/j.fct.2017.08.029.
[27] G. Yang, L. Zhang, L. Ma, R. Jiang, G. Kuang, et al., Glycyrrhetinic acid prevents acetaminophen-induced acute liver injury via the inhibition of CYP2E1 expression and HMGB1-TLR4 signal activation in mice, Int. Immunopharmacol. 50 (2017) 186–193, https://doi.org/10.1016/j.intimp.2017.06.027.
[28] L. Ji, T. Liu, Y. Chen, Z. Wang, Protective mechanisms of N-acetyl-cysteine against pyrrolizidine alkaloid clivorine-induced hepatotoxicity, J. Cell. Biochem. 108 (2009) 424–432, https://doi.org/10.1002/jcb.22269.
[29] J.E. Laine, S. Auriola, M. Pasanen, R.O. Juvonen, Acetaminophen bioactivation by human cytochrome P450 enzymes and animal microsomes, Xenobiotica 39 (2009) 11–21, https://doi.org/10.1080/00498250802512830 the fate of foreign compounds in biological systems.
[30] J.L. Raucy, J.M. Lasker, C.S. Lieber, M. Black, Acetaminophen activation by human liver cytochromes P450IIE1 and P450IA2, Arch. Biochem. Biophys. 271 (1989) 270–283, https://doi.org/10.1016/0003-9861(89)90278-6.
[31] S.I. Adachi, K.I. Nihei, Y. Ishihara, F. Yoshizawa, K. Yagasaki, Anti-hyperuricemic effect of taxifolin in cultured hepatocytes and model mice, Cytotechnology 69 (2017) 329–336, https://doi.org/10.1007/s10616-016-0061-4.
[32] X. Li, H. Xie, Q. Jiang, G. Wei, L. Lin, et al., The mechanism of (+) taxifolin's protective antioxidant effect for *OH-treated bone marrow-derived mesenchymal stem cells, Cell. Mol. Biol. Lett. 22 (2017) 31, https://doi.org/10.1186/s11658-017-0066-9.
[33] Y.H. Liu, Q.H. Huang, X. Wu, J.Z. Wu, J.L. Liang, et al., Polydatin protects against acetaminophen-induced hepatotoxicity in mice via anti-oxidative and anti-apoptotic activities, Food Funct. 9 (2018) 5891–5902, https://doi.org/10.1039/c8fo01078a.
[34] J. Porteous, L. Cioccari, P. Ancona, E. Osawa, K. Jones, et al., The outcome of acetaminophen-induced acute liver failure managed without intracranial pressure monitoring or transplantation, Liver Transplant. : Off. Publ. Am. Assoc. Stud. Liver Di. In. Liver Transplant. Soc. (2018), https://doi.org/10.1002/lt.25377.
[35] R. Brigelius-Flohe, M. Maiorino, Glutathione peroxidases, Biochim. Biophys. Acta 1830 (2013) 3289–3303, https://doi.org/10.1016/j.bbagen.2012.11.020.
[36] Y. Higashi, A. Pandey, B. Goodwin, P. Delafontaine, Insulin-like growth factor-1 regulates glutathione peroxidase expression and activity in vascular endothelial cells: implications for atheroprotective actions of insulin-like growth factor-1, Biochim. Biophys. Acta 1832 (2013) 391–399, https://doi.org/10.1016/j.bbadis.2012.12.005.
[37] S.M. Tan, N. Stefanovic, G. Tan, J.L. Wilkinson-Berka, J.B. de Haan, Lack of the antioxidant glutathione peroxidase-1 (GPx1) exacerbates retinopathy of prematurity in mice, Investig. Ophthalmol. Vis. Sci. 54 (2013) 555–562, https://doi.org/10.1167/iovs.12-10685.
[38] V. Gouaze, N. Andrieu-Abadie, O. Cuvillier, S. Malagarie-Cazenave, M.F. Frisach, et al., Glutathione peroxidase-1 protects from CD95-induced apoptosis, J. Biol. Chem. 277 (2002) 42867–42874, https://doi.org/10.1074/jbc.M203067200.
[39] P.D. Josephy, Genetic variations in human glutathione transferase enzymes: significance for pharmacology and toxicology, Hum. Genom. Proteom. : HGP 2010 (2010) 876940, https://doi.org/10.4061/2010/876940.
[40] H.J. Atkinson, P.C. Babbitt, Glutathione transferases are structural and functional outliers in the thioredoxin fold, Biochemistry 48 (2009) 11108–11116, https://doi.org/10.1021/bi901180v.
[41] J. Zhang, T. Hosoya, A. Maruyama, K. Nishikawa, J.M. Maher, et al., Nrf2 Neh5 domain is differentially utilized in the transactivation of cytoprotective genes, Biochem. J. 404 (2007) 459–466, https://doi.org/10.1042/BJ20061611.
[42] J. Huang, Y. Jia, Q. Li, K. Son, C. Hamilton, et al., Glutathione content and expression of proteins involved with glutathione metabolism differs in longissimus dorsi, subcutaneous adipose, and liver tissues of finished vs. growing beef steers, J. Anim. Sci. 96 (2018) 5152–5165, https://doi.org/10.1093/jas/sky362.
[43] M.N. Hasan, Z. Akond, M.J. Alam, A.A. Begum, M. Rahman, et al., Toxic dose prediction of chemical compounds to biomarkers using an ANOVA based gene expression analysis, Bioinformation 14 (2018) 369–377, https://doi.org/10.6026/97320630014369.